GE

Approved for public release; distribution unlimited.



| 1. AGENCY USE ONLY (Leave blank) | 2. REPORT DATE | 3. REPORT TYPE AND DATES COVERED |
|---|---|---|
| | | FINAL 11 Sep 90 TO 10 Sep 93 |

**4. TITLE AND SUBTITLE**
MODELS OF THE NEURONAL MECHANISMS OF TARGET LOCALIZATION OF THE BARN OWL

**5. FUNDING NUMBERS**
F49620-89-C-0131
61102F
2313
CS

**6. AUTHOR(S)**
John Pearson

**7. PERFORMING ORGANIZATION NAME(S) AND ADDRESS(ES)**
David Sarnoff Research Center
201 Washington Road
Princeton, NJ 08543-5300

**8. PERFORMING ORGANIZATION REPORT NUMBER**
AFOSR-TR- 94 0061

**9. SPONSORING/MONITORING AGENCY NAME(S) AND ADDRESS(ES)**
AFOSR/NL
110 Duncan Avenue, Suite B115
Bolling AFB DC 20332-0001

**10. SPONSORING/MONITORING AGENCY REPORT NUMBER**




**11. SUPPLEMENTARY NOTES**

**12a. DISTRIBUTION/AVAILABILITY STATEMENT**

Approved for public release;
distribution unlimited

**12b. DISTRIBUTION CODE**

**13. ABSTRACT** *(Maximum 200 words)*

Models of the computation of sound direction in the brainstem and midbrain of the barn owl (tyto alba) were developed. Nucleus laminaris is the first site of interaural time-delay (ITD) processing. It was shown that standard neuron models would have to have unrealistically fast time constants in order to match the 10 micro-second ITD resolution characteristic of laminaris neurons. Three physiological reasonable, qualitatively distinct alternatives, were developed. Nucleus ventralis lemnisci lateralis pars posterior (VLVp) and the lateral shell of the central nucleus of the inferior colliculus (ICL) are the first two stages of interaural level differences (ILD) processing. It was shown how a "thermometer" code of ILD could be formed in VLVp through competitive dynamics, and how the ILD-tuned responses of ICL neurons could derive from the VLVp through lateral inhibition. It was shown how this architecture could be modified to achieve near independence from the average binaural level. Experimentalists are now checking the predictions of these models of ILD and ITD processing.

| 14. SUBJECT TERMS | | | 15. NUMBER OF PAGES |
|---|---|---|---|
| | | | 16. PRICE CODE |
| 17. SECURITY CLASSIFICATION OF REPORT | 18. SECURITY CLASSIFICATION OF THIS PAGE | 19. SECURITY CLASSIFICATION OF ABSTRACT | 20. LIMITATION OF ABSTRACT |
| (U) | (U) | (U) | (UL) |

NSN 7540-01-280-5500

Standard Form 298 (Rev. 2-89)
Prescribed by ANSI Std. 239-18
298-102

# Models of the Neuronal Mechanisms of Target Localization of the Barn Owl

John Pearson, Project Director
David Sarnoff Research Center
Princeton, N.J. 08543-5300

November 1993

Final Technical Report

Contract No.: F49620-89-C-0131

Air Force
Office of Scientific Research

## A. BACKGROUND

Most of the visual, auditory, and somatosensory nuclei of the central nervous system exhibit map-like architectures, in which neuronal response characteristics exhibit a systematic spatial variation over the nucleus. These map-like nuclei appear to serve as modules within hierarchical and parallel computing systems. These systems are examples of how to break large, complex problems down into smaller, simpler sub-problems, and an understanding of them may provide insight into the construction of similarly powerful solutions in the technological domain. In addition, they exhibit other useful properties for man-made computing systems, such as self-organization, self-optimization, and fault-tolerance. The neural substrate for target localization in the barn owl is one such system.

The barn owl can hunt in total darkness, recognizing and locating prey by hearing alone. One component of this behavior is a very accurate head-orienting response to salient sounds (the head must rotate as the eyes are immobile). This head saccade centers the sound-producing object for *closer visual and acoustic scrutiny, prior* to aerial attack. In the laboratory, owls can be trained to produce naturalistic head saccades to controlled sounds, and thus indicate the perceived sound location. In this way, the barn owl has been shown to be more accurate at localizing sounds than any other terrestrial animal studied thus far [12].

Considerable progress has been made in determining the acoustic and neural bases of the head saccade (see Fig. 1). The following description is greatly simplified, as its purpose is limited to providing the context for the work reported here (see [15, 7] for recent reviews). The acoustical properties of the owl's head and ears lead to the encoding of stimulus azimuth and elevation by interaural time delay (ITD) and interaural level difference (ILD), respectively [18]. In effect, associated with each direction in space there is a unique relationship between frequency (F), ITD, and ILD; to determine the direction of a sound source, the system must, in effect, compute the nonlinear mapping between the ITD and ILD spectrum of the sound and its direction.

The binaural ITD and ILD information is extracted in two steps. First the monaural timing and intensity information are separated by the cochlear nuclei [26]. Second, maps representing the

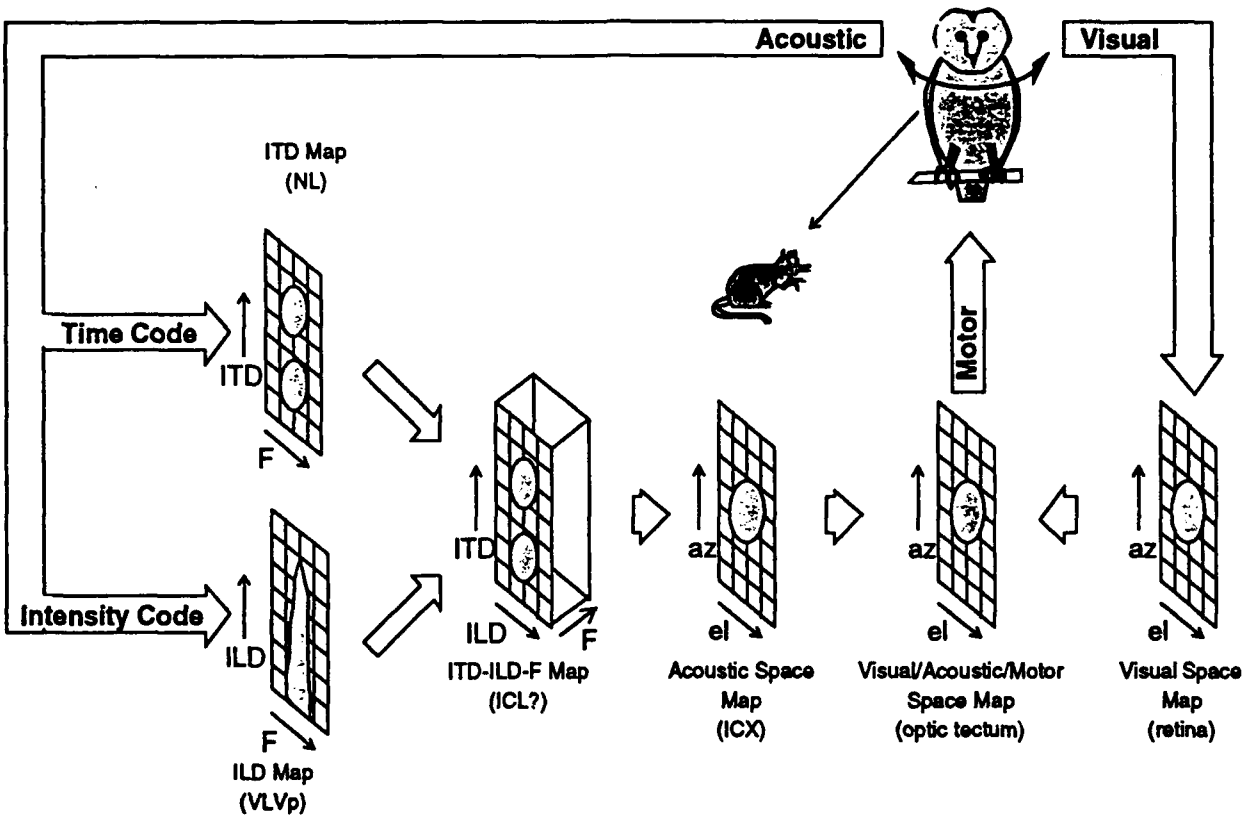


**Fig. 1** Overview of the neural system for auditory localization in the barn owl. The grids indicate the map-like representation of information at each processing stage or nucleus. The "blobs" indicate the pattern of neuronal activation on the map in response to a typical stimulus. Acronyms NL, VLVp, ICL, ICX, ITD, and ILD are defined in the text. Arrows indicate the direction of signal flow. Symbols "az" and "el" denote azimuth and elevation, respectively, while F denotes frequency.

ITD [27] and ILD [16] spectra are produced in, respectively, nucleus laminaris (NL) and the nucleus ventralis lemnisci lateralis pars posterior (VLVp).

Our previous modeling (prior to the start of this contract) suggested that the merger of ITD and ILD should occur in two stages, in order to avoid the problem of phantom targets in multi-sound environments [22]. In the first stage, presumably the lateral shell of the central nucleus of the inferior colliculus (ICL), cells are tuned to unique combinations of ITD, ILD, and frequency, and arranged in a three-dimensional map. In the second stage, each of the ICL neurons projects to and excites the region of the space map in the ICX that corresponds to the direction associated with the ITD/ILD/F triplet to which it is tuned. Recent experimental work is in basic agreement with this model [4], but many details remain to be worked out. In any case, the equivalent of an "acoustic retina" is found in the external nucleus of the inferior colliculus (ICX) [13, 14].

In the optic tectum, projections from the ICX [10] and the retina produce a fused visual-acoustic representation of target direction [11], and both sensory maps are in register with a motor map of head saccade vector [3]. The visual/auditory alignment must be dynamically adjusted while the head is growing, because the changing shape of the head alters the relationship between ITD, ILD, frequency, and sound direction. The tectal auditory map shifts so as to stay in alignment with the tectal visual map [6, 8, 9]. This could easily be explained by correlation-driven synaptic plasticity acting within a one-to-many ICX-to-tectum projection, and we in fact proposed such a model [19, 5]. However, current work in the Knudsen lab is demonstrating that the plasticity is upstream of the tectum, in the inferior colliculus [1, 17]. This implies that the visual feedback must be indirect, as there are no known visual sensory inputs to the inferior colliculus.

## B. OBJECTIVES

The purpose of this project was to further the understanding of this system through the development of biophysical and computational models and computer simulations. The near-term goal of this work was to produce explicit, testable predictions for neuroscience. In addition, it is expected that this research will lead to new artificial neural network designs, with applications for signal processing, sensory fusion, and sensorimotor integration.

## C. RESEARCH RESULTS

### 1. Modeling the Intensity System

Instead of modeling the ICL-to-ICX projection and visual/auditory plasticity, as originally proposed, we chose to model the intensity processing system in the VLVp and ICL. This change was made for several reasons in response to experimental reports made after the proposal was written. Fujita [4] reported that the ICL contained both ILD-tuned and ILD-sensitive neurons, and that there was some convergence across frequency in the ICL. Our previous model of the ICL incorporated only ILD-tuned cells and had no frequency convergence. Therefore it was decided to first construct a model of the ICL that could account for these findings before using it to model the

formation of the space map in the ICX and visual/auditory fusion. This of course requires models of the inputs to the ICL. The nature of the representation of ITD prior to the ICL was quite well understood, however the representation of intensity and ILD prior to the ICL was not. However, the publication of Carr's anatomical study of the VLVp [2], along with Manley's physiological paper [15], gave us enough information to attempt a model and simulation of the VLVp. Therefore, we decided to develop joint models of the intensity processing of the VLVp and the ICL.

The first version of the network model of VLVp was presented at NIPS in December 1989 [23]. Subsequent discussions with experimentalists informed us of their latest unpublished results, which called for significant revisions at the level of the detailed anatomy, although the basic computational model remained the same. The second version of the VLVp model was presented at the first meeting of the AMNS Workshop [24].

The next phase of the research was to revise the network model of the ICL. We were joined in this work by a new collaborative experimentalist, Ralph Adolphs of CalTech. Ralph kept us informed of the latest findings in his and other barn owl labs. Of special relevance was his own work in which various neural activity modulators were injected into the VLVp and the effects on stimulus response recorded in the VLVp and ICX. The next ICL paper, presented at the 2nd AMNS workshop, included simulations of Ralph's experiments [28] (see also appendix).

Within the last year Ralph published detailed anatomical tracing studies [30] which suggest that the inter-VLVp inhibition is feedforward, rather than feedback, as it was assumed to be in our first model [28]. This finding contradicts earlier work by Takahashi [33], whose HRP tracings were consistent with the feedback model. In any case, we decided to explore whether a feedforward model could match the data of Manley et. al. [16] as well as the feedback model did. Our approach to this question was to train a static network to match the steady-state output of our dynamic feedback model, using the techniques developed in the field of artificial neural networks. Work just completed demonstrates that the synaptic weights can be adjusted so that the response curves are very similar to those of the original feedback model. However, a few of the ventral

neurons in the feedforward model have response characteristics which do not match those found in the VLVp. The feedback model is a closer match to the known anatomy in several other ways, and is at present still the best candidate, in our opinion. More anatomical experiments will have to be done to distinguish between which of these models is correct. This is somewhat surprising, since the dynamics of the two models are so intrinsically different. This work was presented at the Society for Neuroscience Annual Meeting this year [32] and a manuscript is in preparation for submission to the Journal of Neuroscience.

Adolph's [30] also presented evidence that the VLVp--> ICL projection is bilateral, with the ipsilateral projection weaker than the contralateral projection. Previous work by Takahashi (unpublished, personal communication, summer 1988) had revealed a contralateral-only projection, and this finding was built into our previous ICL modeling. Conceptually, the presence of a bilateral projection does not invalidate our previous model, and in fact, bilateral projections could be incorporated in such a way that the resulting ICL responses and the underlying computational model ("spatial derivative model") would be the same. However, a bilateral projection does provide more degrees of freedom, and we were interested if perhaps an entirely different computational scheme could be implemented using it.

We were especially interested in deriving a new model of the VLVp --> ICL projection for which the dependence on the average binaural intensity (ABI) would be less in the ICL than in the VLVp. Our previous ICL model [28] was just as dependent on ABI as the VLVp. This is because the underlying spatial derivative model is based on point-to-point, topographic projections, and so the ICL must inherit the same degree of ABI dependence as the VLVp. The degree to which neurons in the ICL, ICX, and optic tectum are independent of ABI has not been extensively studied. It has generally been maintained that ICX and tectal cells are relatively independent of ABI [7], and this is what one would expect, since these neurons are thought to encode sound source direction, which is of course independent of ABI. However, there is also evidence from Olsen et al. [31] that tectal cells show the same kind of dependence on ABI that VLVp cells do [16].

Our approach was to use the training methods of artificial neural networks to derive the connections between the VLVp and the ICL, as well as those within the ICL. We found that nearly ABI independent cells can be produced in the ICL. However, the ipsilateral projection from the VLVp was not essential for this. Models with the full bilateral projection were slightly more ABI independent than those with a contralateral-only projection, but the difference was not large. As expected, analysis of the resulting trained network revealed that it is based on a different computational scheme than the spatial-derivative model. Rather than being point-to-point, the projection onto a ICL neuron comes from a wide region of the VLVp. ABI independence is achieved through a balancing act between excitation and inhibition. So we have found one way in which ABI independence can be achieved. Experimental work is needed to measure the actual degree of ABI independence. This work was presented at the CNS Conference this summer, at the Society for Neuroscience Annual Meeting this year [32], and a manuscript is in preparation for submission to the Journal of Neuroscience.

## 2. Modeling Time Delay Hyperacuity in Nucleus Laminaris

The auditory system of the barn owl contains neurons sensitive to the phase of sounds of remarkably high frequency, up to 9 kHz. Nucleus Laminaris (NL) represents phase differences as part of the computation of stimulus azimuth [27]. The input to NL is from both of the monaural magnocellular nuclei (NM). NM neurons encode stimulus phase or time by firing action potentials preferentially near a particular phase of the stimulus [26]. However, there is significant jitter in the phase at which the action potentials occur, which is noise in the input to NL. Furthermore, NM neurons cannot fire during every period of the sound at such high frequencies, so the number of spikes arriving at a laminaris neuron from each side of the head varies considerably from one sound period to the next, giving an additional source of noise. The high frequency of the stimulus and the high level of noise in the input spike trains make the response properties of laminaris neurons hard to explain, and casts doubt on the common picture of NL neurons as coincidence detectors. We used simulations and semi-numerical analysis to show that the cellular and synaptic

time constants must be very fast, probably unreasonably so, in order for ordinary biophysical mechanisms to reproduce the observed behavior.

Several people have suggested that a resonance mechanism may exist in laminaris neurons to amplify the signal. We investigated a simple neuronal resonance model that improved the performance considerably, but the synaptic and cellular time constants still had to be very fast, and we did not propose a specific biophysical resonance mechanism. This work was published in the proceedings of the second AMNS Workshop [29].

There is one peculiar feature of NL which may explain its ability to deal with high frequencies. In the presence of a sound, there is an extra-cellular potential in NL which oscillates in phase with the sound. This is called the neurophonic potential. Its exact amplitude has not been measured, but it may be in the range of one to ten millivolts [Ted Sullivan, personal communication]. The most likely sources of the neurophonic are the NM axons, which are carrying phase-locked spikes whose external fields would add coherently. This signal has relatively little noise simply because it is an average over thousands of the noisy signals from individual NM axons. We have calculated how a passive model of an NL neuron with the experimentally-observed cell morphology would respond to such an oscillating external potential. In essence, the cell acts like an electrode. The membrane at the cell body conducts very well at frequencies above five kHz, and the myelinated axon's membrane does not. The oscillating potential near the soma propagates through the soma's membrane and down the axon. As a result, the oscillating part of the potential difference across the membrane is quite small at the soma, but grows in magnitude to a maximum of significant size at some distance down the axon. Voltage-dependent channels respond to the potential difference, so if they can respond at these frequencies they can respond to the oscillating potential difference. This would be a much cleaner signal than the synaptic input from NM.

This model has two appealing features: 1) The computation of potential difference has very few assumptions. The only unknowns are the magnitude of the external potential and the ability

of the neuron to fire in response to the high-frequency potential difference. The first of these unknowns needs to be addressed experimentally, the second can be investigated through simulations. 2) The model provides an explanation for the unusual appearance of NL neurons in electron micrographs, especially the lack of a spike-initiating zone at the beginning of the axon. These observations were made by Catherine Carr, who suggested that spikes may be initiated at the first node in the axon, but there was no known reason for the neurons to have this structure. A manuscript is in preparation for publication in the Journal of Neuroscience.

### 3. Other Related Work

In addition to his role as consultant to the research effort at Sarnoff, Dr. Sullivan pursued a number of neurocomputational research topics related to the theme of this contract. The following is his report.

Past work by myself an others had shown that the processing of information about stimulus timing and intensity are physically separated, and that neurons in the brainstem regions responsible for these two functions are anatomically distinct. However, while we know a lot about the anatomy and physiology of neurons in both the time and intensity pathways, we have a poor understanding of the reasons for the relationship between a neuron's anatomical structure and its physiological functionl. In my work on the auditory brainstem, I have found that questions of structure-function interrelationships are best approached in systems for which the physiological function of a particular neuron is fairly well understood. That is, it is easier to ask why a cell with a specific processing function has a particular anatomical structure than it is to ask what the function of a given cell with a known structure might be. I have used this approach to investigate the possible role of dendritic processes in neurons which compute horizontal sound localization by measurement of interaural time differences and to examine what advantages dendrites might provide to neurons specialized for processing information about stimulus intensity. In these studies and others designed to investigate physiological mechanisms of both time and intensity processing, I have come to realize more clearly that the physiological mechanisms available to optimize

selectivity in the time domain are drastically different and often diametrically opposed to those which work best for intensity. My work is beginning to provide clear physiological explanations for the functional segregation that is observed in the auditory system and suggests that an understanding of cellular mechanisms can also help to explain higher levels of neuronal organization as well. The time and intensity segregation seen in the auditory system can also provide insights into the similar organization of other sensory systems since for any sense for which the stimulus is a form of energy (e.g. sound, light, touch), both the spatial pattern of energy distribution (i.e. intensity) across the sensory receptors and the temporal pattern changes in this distribution must be neurally encoded

Dendritic function in nucleus laminaris:

I have refined and extended a model for dendritic function in binaural time comparison. Earlier theoretical and empirical work has established that this computation involves a cellular process called coincidence detection in which a cell's spike output depends on its receiving at least two separate, temporally synchronized synaptic inputs. Neurons which perform this task at low frequencies have a pair of long dendrite, each dendrite being innervated by synaptic inputs derived from the ear opposite to those impinging on the other dendrite. The modeling results suggest that these bipolar dendrites enhance the cell's selectivity for simultaneous inputs impinging on both dendrites as compared to coincidences of two inputs arriving on the same side. This function requires electrical isolation between the synaptic inputs from the two ears and therefore cannot be done without dendrites. However, the mechanism exploits a fundamental property of neuronal synaptic transmission (voltage saturation) and is therefore a general candidate for dendritic functions involving sensitivity or selectivity for specific spatial or temporal combinations of synaptic input. Further analysis of the model's predictions using more realistic periodic synaptic inputs shows that aspects of dendritic morphology such as length, branching patterns and number can be understood in the context of the basic mechanism I am proposing.

Comparison of binaural phase processing at high and low frequencies:

Anatomical and physiological evidence indicates that the possible mechanisms of binaural time comparison which I have described do not (and in fact can not) operate in neurons which perform this task at high frequencies (>5000 cycles/sec) in the barn owl. These cells have no dendrites and also have a different axon morphology. A large portion of the work was devoted to understanding the physiological process which can enable timing information to be extracted from signals whose time course is much faster that what is normally considered for neuronal processes. My investigations show that both the temporal properties of synaptic input (transmitter release, post-synaptic change in electrical properties) and the mechanisms of spike output need to be examined and that with modest changes in both of these areas, the function of these cells can be explained. Most recently, I have been studying the relationship between the stochastic behavior of the action potentials in the input neurons and the patterns of synaptic conductance change seen by the coincidence detector cells. These ongoing studies are providing some interesting and insightful results that should help to confirm the functional/physiological dichotomy between temporal and level (intensity) processing mechanisms discussed above.

Cellular mechanisms of intensity processing in nucleus angularis:

I have applied a similar logic to the one used to investigate time comparison mechanisms to an analysis to dendritic function in the processing of stimulus intensity. In this case, I have concluded that some of the intensity averaging functions which had been thought to be done by dendrites are not likely to be what dendrites are for since these functions can be done more efficiently in an adendritic cell. Rather, I am proposing a novel dendritic function for these cells: enhancement of the dynamic range of synaptic strength between threshold and saturation. This and other work that I have done suggests that the comparison of optimal morphological parameters obtained with different assumption about function is likely to provide a powerful approach to both the theoretical and empirical investigation of interactions between anatomy and physiology. I have begun a collaboration with Dr. Cathrine Carr at the University of Maryland designed to test some of the predictions of this work.

## D. PUBLICATIONS


1. Pearson, J.C., C.D. Spence and R. Adolphs, "Model of the Origin of Neuronal Selectivity for Binaural Intensity Difference in the Barn Owl", *Neural Systems: Analysis and Modeling*, F. Eeckman, ed, Kluwer, Boston (1993). (See Appendix).
2. Spence, C.D. and J.C. Pearson, "A Resonance Model of High Frequency Binaural Phase Sensitivity in the Barn Owl Auditory Brainstem", *Neural Systems: Analysis and Modeling*, F. Eeckman, ed, Kluwer, Boston (1993). (Included in the Appendix of the November 1991 Annual Report).
3. Pearson, John C., and Spence, Clay D., "Back-Propagation Generation of Hypotheses For The Projection Patterns Which Give Rise to Neurons Tuned To Interaural Level Differences In The Barn Owl's Midbrain", *Society for Neuroscience Abstracts*, Volume 19, pp. 530 (1993).
4. Spence, C. D., and J. C. Pearson, "Models of the computation of sound elevation in the barn owl," *Analysis and Modeling of Neural Systems*, F.Eeckman, ed, Kluwer, Boston (1992). (Included in the Appendix of the December 1990 Annual Report).
5. Pearson, John C., and Spence, Clay D., "A Resonance Model of Microsecond Time Sensivity in Nucleus Laminaris of the Barn Owl", *Society for Neuroscience Abstracts*, Volume 17, Part I, pp. 306 (1991).
6. Pearson, J. C., C. D. Spence, and R. Adolphs, "The computation of sound elevation in the barn owl: model and physiology," *Society for Neuroscience Abstracts* **16** (299.3), 718 (1990).
7. Pearson, J. C., and C. D. Spence, "Model of the computation of auditory stimulus direction and tuning to interaural level difference in the inferior colliculus of the barn owl," *Society for Neuroscience Abstracts* **15** (50.6),114 (1989).
8. Spence, C. D., and J. C. Pearson, "The computation of sound source elevation in the barn owl," *Advances in Neural Information Processing Systems 2*, edited by D. S. Touretzky (Morgan Kaufmann, San Mateo, CA, 1990), pp. 10-17. (Included in the Appendix of the December 1990 Annual Report).
9. Sullivan, W.E. "Horizontal sound localization at high and low frequencies: The biophysics of structure-function correlations in nucleus laminaris" *Computational Neural Systems 1992 Symposium book*, (1992) (In press).
10. Sullivan, W.E. (1991) Possible mechanisms of high frequency phase comparison in barn owls. *Society Neuroscience Abstracts* 17: 446 (1992).
11. Sullivan, W. E., "Resolution of μsec timing in a neural compartmental model," *Society for Neuroscience Abstracts* **16** (360.3), 871 (1990).
12. Sullivan, W.E., "Temporal Hyperacuity and single neuron selectivity: Microsecond time resolution in a neural compartmental model", *Journal of Comparative Physiology* (Being Revised).
13. Sullivan, W.E. "Modeling high-frequency interaural phase comparison in nucleus laminaris of the barn owl", *Journal of Neuroscience* (Submitted).

## E. REFERENCES


1. Brainard, M. S. and E. I. Knudsen, "The inferior colliculus is a site of plasticity in the visual calibration of auditory spatial tuning in developing barn owls," *Society for Neuroscience Abstracts* **16**, 828 (1990).
2. Carr, C. E., I. Fujita, and M. Konishi, "Distribution of GABAergic neurons and terminals in the auditory system of the barn owl," *The Journal of Comparative Neurology* **286**, 190-207 (1989).
3. du Lac, S. and E. I. Knudsen, "Neural maps of head movement vector and speed in the optic tectum of the barn owl," *Journal of Neurophysiology*, **63**, 131-146 (1990).
4. Fujita, I., and M. Konishi, "Transition from single to multiple frequency channels in the processing of binaural disparity cues in the owl's midbrain," *Society for Neuroscience Abstracts* **15**, 114 (1989).
5. Gelfand, J. J., J. C. Pearson, C. D. Spence and W. E. Sullivan, "Multisensor integration in biological systems," *Proceedings of the Third IEEE Symposium on Intelligent Control*, (1988).
6. Knudsen, E. I. and M. S. Brainard, "Vision instructs the auditory spatial tuning of neurons in the optic tectum of developing barn owls," *Society for Neuroscience Abstracts* **16**, 828 (1990).
7. Knudsen, E. I., S. du Lac and S. Esterly, "Computational maps in the brain," *Annual Review of Neuroscience*, **10**, 41-65 (1987).
8. Knudsen, E. I., "Experience alters the spatial tuning of auditory units in the optic tectum during a sensitive period in the barn owl," *Journal of Neuroscience*, **5**, 3094-3109 (1985).
9. Knudsen, E.I. and P. F. Knudsen, "Vision guides the adjustment of auditory localization in young barn owls," *Science*, **230**, 545-548 (1985).
10. Knudsen, E. I., and P. F. Knudsen, "Space-mapped auditory projections from the inferior colliculus to the optic tectum in the barn owl (*Tyto alba*)," *Journal of Comparative Neurology*, **218**, 187-196 (1983).
11. Knudsen, E. I., "Auditory and visual maps of space in the optic tectum of the owl," *Journal of Neuroscience*, **2**, 1177-1194 (1982).
12. Knudsen, E. I., G. G. Blasdel and M. Konishi, "Sound localization by the barn owl (Tyto alba) measured with the search coil technique," *The Journal of Comparative Physiology*, **133**, 1-11 (1979).
13. Knudsen, E.I. and M. Konishi, "A neural map of auditory space in the owl," *Science*, **200**, 795-797 (1978).
14. Knudsen, E.I. and M. Konishi, "Space and frequency are represented separately in auditory midbrain of the owl," *Journal of Neurophysiology*, **41**, 871-884 (1978).
15. Konishi, M., "Centrally synthesized maps of sensory space," *Trends in Neuroscience*, **9**, 163-168 (1986).
16. Manley, G. A., C. Koppl, and M. Konishi, "A neural map of interaural intensity differences in the brain stem of the barn owl," *The Journal of Neuroscience* **8**(8), 2665-2676 (1988).

17. Mogdans, J. and E. I. Knudsen, "Auditory experience modifies the tuning for sound localization cues of neurons in the barn owl's optic tectum and inferior colliculus," *Society for Neuroscience Abstracts* **16**, 828 (1990).

18. Moiseff, A., "Binaural disparity cues available to the barn owl for sound localization," *Journal of Comparative Physiology*, **164**, 629-636 (1989).

19. Pearson, J. C., J. J. Gelfand, W. E. Sullivan, R. M. Peterson, and C. D. Spence, "Neural network approach to sensory fusion," C. B. Weaver, ed. SPIE **931**, 103-108 (1988).

20. Pearson, J. C., and C. D. Spence, "Model of the computation of auditory stimulus direction and tuning to interaural level difference in the inferior colliculus of the barn owl," *Society for Neuroscience Abstracts* **15** (50.6), 114 (1989).

21. Pearson, J. C., C. D. Spence, and R. Adolphs, "The computation of sound elevation in the barn owl: model and physiology," *Society for Neuroscience Abstracts* **16** (299.3), 718 (1990).

22. Spence, C. D., J. C. Pearson, J. J. Gelfand, R. M. Peterson and W. E. Sullivan, "Neuronal maps for sensory motor control in the barn owl," *Advances in Neural Information Processing Systems 1*, edited by D. S. Touretzky (Morgan Kaufmann, San Mateo, CA, 1988), 366-374.

23. Spence, C. D., and J. C. Pearson, "The computation of sound source elevation in the barn owl," *Advances in Neural Information Processing Systems 2*, edited by D. S. Touretzky (Morgan Kaufmann, San Mateo, CA, 1990), 10-17.

24. Spence, C. D., and J. C. Pearson, "Models of the computation of sound elevation in the barn owl," *Proceedings of the Analysis and Modeling of Neural Systems Workshop*, Berkeley, CA (in press).

25. Sullivan, W. E., "Resolution of μsec timing in a neural compartmental model," *Society for Neuroscience Abstracts* **16** (360.3), 871 (1990).

26. Sullivan, W. E. and M. Konishi, "Segregation of stimulus phase and intensity coding in the cochlear nucleus of the barn owl," *Journal of Neuroscience*, **4**, 1787-1799 (1984).

27. Sullivan, W. E. and M. Konishi, "Neural map of interaural phase difference in the owl's brainstem," *Proceedings of the National Academy of Sciences USA*, **83**, 8400-8404 (1986).

28. Pearson, J.C., C.D. Spence and R. Adolphs, "Model of the Origin of Neuronal Selectivity for Binaural Intensity Difference in the Barn Owl", *Neural Systems: Analysis and Modeling*, F. Eeckman, ed., Kluwer, Boston (1993).

29. Spence, C.D. and J.C. Pearson, "A Resonance Model of High Frequency Binaural Phase Sensitivity in the Barn Owl Auditory Brainstem", *Neural Systems: Analysis and Modeling*, F. Eeckman, ed., Kluwer, Boston (1993).

30. Adolphs, Ralph, "Bilateral Inhibition Generates Neuronal Responses Tuned to Interaural Level Differences in the Auditory Brainstem of the Barn Owl", *Journal Of Neuroscience*, 13, 3647-3668 (1993).

31. Olsen, John F., Knudsen, Eric I. and Esterly, Steven D., "Neural Maps of Interaural Time and Intensity Differences in the Optic Tectum of the Barn Owl", *Journal of Neuroscience*, 9, 2591-2605 (1989).

# APPENDIX A

## Model of the Origin of Neuronal Selectivity for Binaural Intensity Difference in the Barn Owl

Published in:

Neural Systems: Analysis and Modeling

Edited by: Frank H. Eeckman

Kluwer (1993)

Published in:

Neural Sustems: Analysis and Modeling
edited by: Frank H. Eeckman
Kluwer (1993)

# Model of the Origin of Neuronal Selectivity for Binaural Intensity Difference in the Barn Owl

J. C. Pearson[1], C. D. Spence[1] and R. Adolphs[2]
[1]David Sarnoff Research Center
Princeton, NJ 08543-5300
[2]Div. of Biology 216-76
CalTech, Pasadena, CA 91125

## Abstract

*A model is presented of the neural computation of binaural intensity difference (BID) in the lateral shell of the central nucleus of the inferior colliculus (ICL) of the barn owl. The ICL is the second stage of binaural intensity processing, following the nucleus ventralis lemnisci lateralis pars posterior (VLVp), and it projects to the external nucleus of the inferior colliculus (ICX). The model shows how monaural excitation from the cochlear nucleus angularis can be combined with inhibition from the VLVp to form a peak-like pattern of activation in the ICL from the wedge-like activation pattern in the VLVp. The model explains the functional roles of the two narrowly frequency-tuned cell types in the ICL, and it predicts their patterns of interconnection. An experiment was performed in which changes in BID selectivity in the ICX were measured following the injection of neural activity modulators into the VLVp. Model simulations of these experiments produce qualitatively similiar results.*

## Overview of Binaural Intensity Processing

Binaural intensity difference (BID) is the strongest cue of elevation for the barn owl (tyto alba) [Moiseff, 1989]. BID varies monotonically with elevation for frequencies above 4 kHz. This is caused by the asymmetrical pattern of dense ruff feathers surrounding the ears [Payne, 1970; Haresign and Moiseff, 1989].

A neural representation of BID is created in several stages, as depicted in Fig. 1. The blocks denote the four main nuclei involved, on both sides of the brain. The

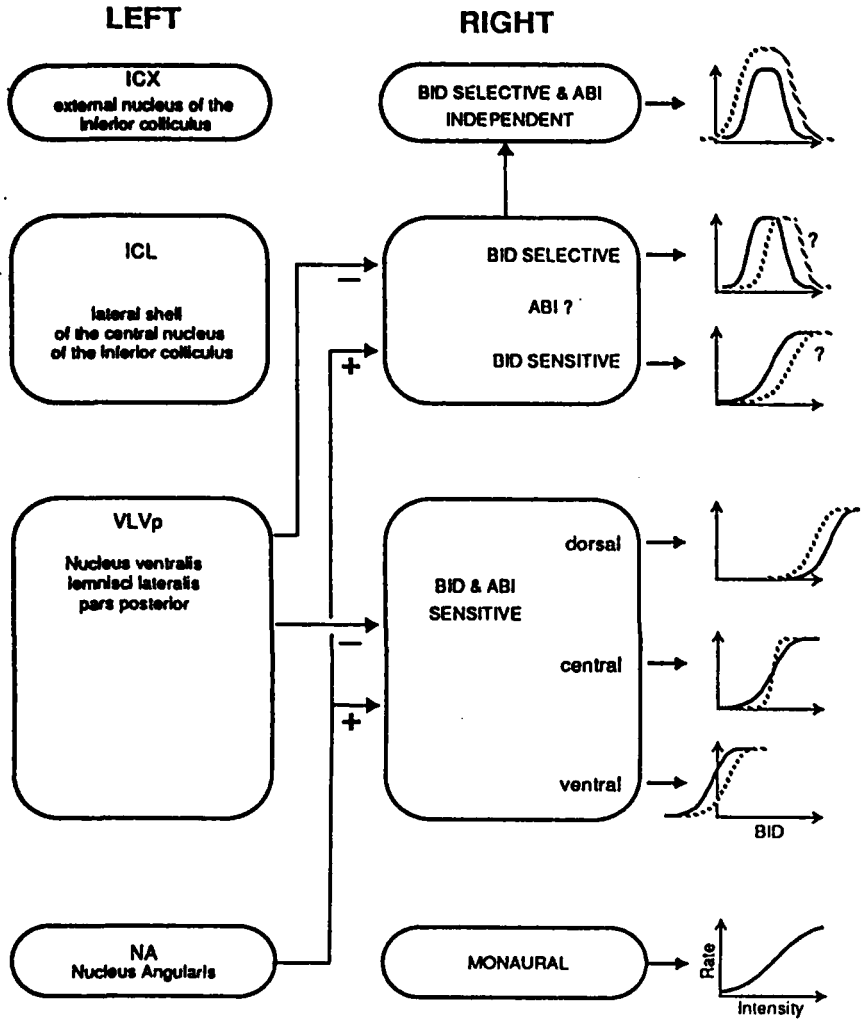


**Fig. 1.** The intensity processing system for sound elevation of the owl.

input to nucleus angularis (NA) (not shown) is from the sensory neurons of the 8th nerve. The names and abbreviations of these nuclei are given in the blocks on the left side, while their response characteristics are summarized on the right side.

NA neurons are monaural, responding only to ipsilateral stimuli within a narrow frequency range. Their firing rate increases montonically with intensity over a 30-50 dB range [Sullivan and Konishi, 1984].



At the other end of the processing stream, ICX neurons are exclusively binaural, firing only to broad-band stimuli with the appropriate BID. ICX neurons are relatively independent of the average binaural intensity (ABI), as their response curves simply broaden with increasing ABI [Knudsen, 1984]. ABI-independence is of course essential for the encoding of sound elevation, because it is principally a function of sound loudness.

The VLVp receives excitatory and inhibitory projections from the contralateral NA [Takahashi and Konishi, 1988] and VLVp [Takahashi, 1988], respectively . VLVp neurons are narrowly tuned in frequency, and are tonotopically arranged along the anterior-posterior axis. VLVp neurons are BID-sensitive, that is, their BID response curve is sigmoidal. This is in contrast to the BID-selective or bell-shaped response curves of ICX neurons. There is a systematic, map-like representation of BID along the dorso-ventral axis. The BID threshold, or BID at which the cell's response is half of its maximum value, decreases linearly from 20dB dorsally to -20dB ventrally. There is no systematic variation of any response characteristic along the medio-lateral axis. A tone of a given frequency and BID will thus excite a ventro-dorsal slab of neurons, the length of which is related to the BID, i.e., a thermometer-like representation of BID. However, VLVp neurons do not accurately represent BID, or sound elevation, as they are also sensitive to ABI. As the ABI is increased, the BID curves of dorsal cells shift to higher BID, those of ventral cells shift in the opposite direction, and those of central cells do not shift but the slope of the curve around threshold decreases [Manley, *et al.*, 1988]. There are three distinct anatomically defined cell classes [Carr, *et al.*, 1989] in the VLVp, however they do not appear to have different stimulus response characteristics.

The next stage in binaural processing is the ICL, which receives projections from the contralateral NA [Takahashi and Konishi, 1988] and VLVp [Takahashi and Konishi, unpublished]. The NA and VLVp inputs are presumably excitatory and inhibitory, respectively, since contralateral stimulation excites ICL neurons, while ipsilateral stimulation inhibits them [R. Adolphs and I. Fujita, unpublished observations]. ICL neurons have properties intermediate between those of the VLVp and the ICX. There are both BID-sensitive cells, as in the VLVp, and BID-selective cells, as in the ICX [Fujita and Konishi, 1989]. All of the BID-sensitive cells and some of the BID-selective cells are narrowly-tuned in frequency, as are VLVp neurons, however some of the BID-selective cells are broadly-tuned, like ICX neurons. The ABI response characteristics of these neurons have not yet been thoroughly investigated, nor has a systematic map of BID-thresholds been discovered. The BID-sensitive and BID-selective neurons are also tuned to binaural time delay which encodes stimulus azimuth. Frequency and binaural time delay are known to be mapped along the dorso-ventral and anterior-posterior axes, respectively [Wagner, *et al.*, 1987].

## Modeling Objective

The objective of this work was to develop a network model of the BID processing of the ICL. The model was designed to produce both the BID-sensitive cell type and the narrowly-tuned (in frequency) BID-selective cell type. The broadly-tuned, BID-selective neurons are not addressed with this model. The model should make predictions concerning the ABI dependence of these two cell types. Of special interest is the ABI dependence of the BID-selective neurons, because they are presumably a major input to the BID-selective, ABI-independent, space specific neurons of the ICX. The model should clarify the functional role of the BID-sensitive cells in the ICL, which is puzzling because this response characteristic already exists in the VLVp. The model should predict the projection patterns of the incoming axons from the VLVp and NA. The model should also be realistic in the time domain, producing stable responses with short stimulus latencies.

## Modeling Approach

The quantitative, mathematical network model of the ICL presented here is based upon an underlying qualitative model of the generation of BID-selectivity, called the "spatial-derivative model". This model, illustrated in Fig. 2, was developed independently by a number of investigators, including S. Volman, T. Takahashi, and the authors of this paper. The spatial-derivative model holds that a tone of a given frequency produces a wedge-like pattern of activation in the VLVp, and that for a fixed ABI, the position of the edge varies roughly linearly with BID. Such a pattern of activation is suggested by the observed dorso-ventral variation of BID-threshold depicted in the graphs of Fig. 1. The model predicts that a peak-like pattern of activation is created along the medio-lateral axis of the ICL, from the wedge-like pattern in the VLVp. The location of the peak of activation would vary roughly linearly with BID, which is clearly consistent with BID-selective responses.

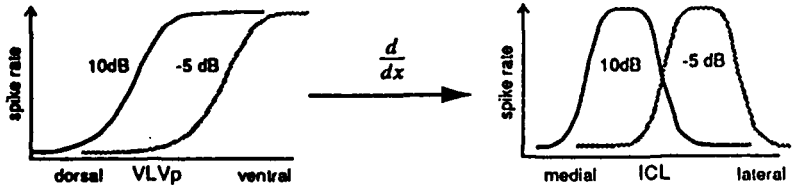


**Fig. 2. The spatial-derivative model of BID-selectivity in the ICL. The curves illustrate the hypothetical activation patterns within the VLVp and ICL for stimuli with BID's of 10dB (solid) and -5dB (grey).**

The degree of biological realism chosen for the model is based upon the objectives stated above, and the level of detail of existing neurophysiological data. The objective is to make predictions at the levels of anatomical connection patterns and qualitative, single cell response characteristics. The level of realism chosen is the same as that used in a previous model of the VLVp [Spence and Pearson, 1991].



The VLVp and ICL are modeled as large networks of discrete, time-dependent, interconnected, spike-producing units. The membrane potential, $v$, is modeled by

$$C\frac{dv}{dt} = -g_L(v-v_L) - g_E(v-v_E) - g_I(v-v_I) \qquad (1)$$

where $v_L$, $v_E$ and $v_I$ are fixed reversal potentials for some set of channels, $g_L$ is a fixed passive leakage conductance, and $g_E$ and $g_I$ are excitatory and inhibitory conductances that are smoothly and linearly driven by incoming spikes in such a way as to approximate the time course of synaptic potentials. Spikes are randomly generated with an average rate given by a sigmoidal function of the membrane potential. (see [Spence and Pearson, 1991] for more detail on the methods of simulation used).

Neural response characteristics are computed as they are in corresponding biological experiments, i.e., through counting the spikes produced to a set of stimuli. Only tone stimuli are considered, as the cells being modeled at this stage are narrowly tuned in frequency.

The VLVp and NA are modeled and simulated in the same way as presented in [Spence and Pearson, 1991]. These models, as depicted in Fig. 3, are briefly summarized here for completeness.

The output from NA is very simply modeled as a constant spike rate that is linearly proportional to the stimulus intensity (5 spikes/ms at 50 dB).

An iso-frequency, dorso-ventral slab of the VLVp is modeled as a network of 1200 neurons (which is close to the actual number in such a slab), divided into 40 clusters of 30 neurons each, defined by their position along the dorso-ventral axis. Three cell types are modeled, as defined by their variation in density along the dorso-ventral axis (as suggested by [Carr, *et al.*, 1989]), and by their inter-connection patterns (as predicted by the model). One class projects in a criss-cross pattern to the contralateral VLVp, and its number density increases from the ventral (18 cells) to the dorsal (2 cells) surface. Another class provides local inhibition, and follows the opposite density gradient. The third class (not shown) is uniformly distributed along the dorso-ventral axis (10 cells in each cluster), and projects to the contralateral ICL. The excitatory input from the contralateral NA is distributed uniformly throughout the slab. For all connections, the strength of individual synapses is independent of dorso-ventral location. However, the cell number gradients effectively create dorso-ventral gradients of inhibition.

This VLVp model reproduces the experimentally measured dorso-ventral distribution of single-unit BID response curves (see Fig. 1, for details see [Spence and Pearson, 1991]), as well as the wedge-like pattern of activation across the VLVp, in

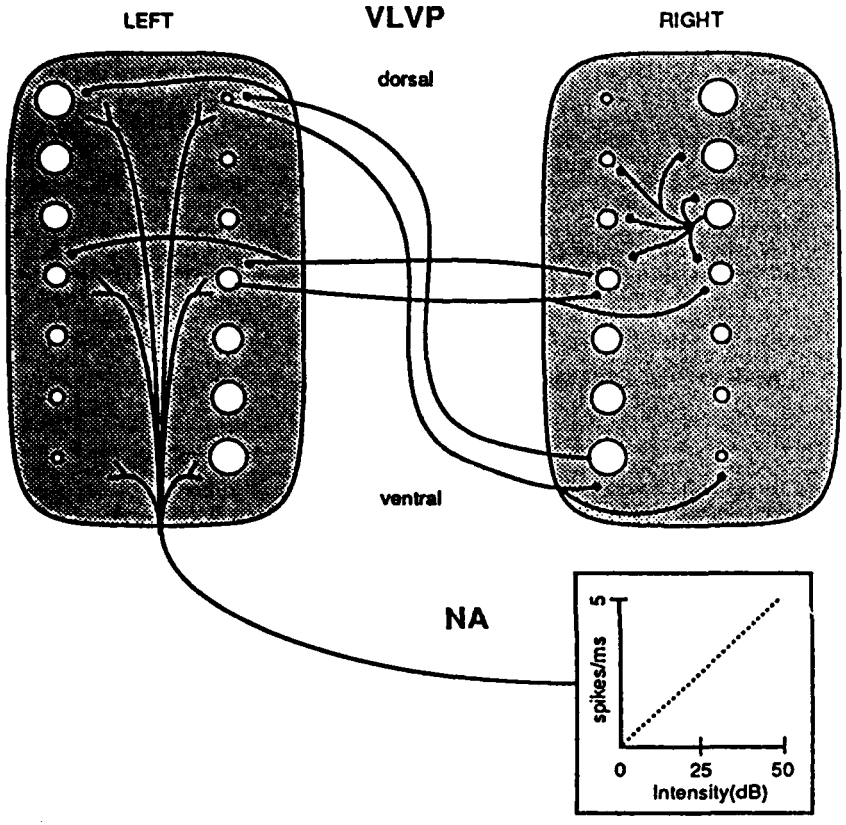


**Fig. 3.** Competitive edge model of the VLVp. The size of the circles denote the number density of the cells of a given type at that position

keeping with the underlying spatial-derivative model (see Fig. 2.). The pattern of dorso-ventral activation for a range of ABI and BID is shown in Fig. 4. Note that increases in ABI compress the range of edge movement, which remains linear (the physiologically relevant range of BID is from -10dB to +20dB).

The wedge-like pattern is the result of a competitive feedback interaction between the criss-cross cell classes of the two VLVp. The cluster with the greatest effective inhibition (roughly the product of NA activation level and cell number) squashes the response of its partner in the other VLVp. The local inhibitory class was found to be essential for insuring the stability and speed of convergence of this feedback process. Interestingly, the three cell classes in the VLVp model have identical response characteristics, due to their having identical input patterns, but unique functional roles, due to their differing output patterns.



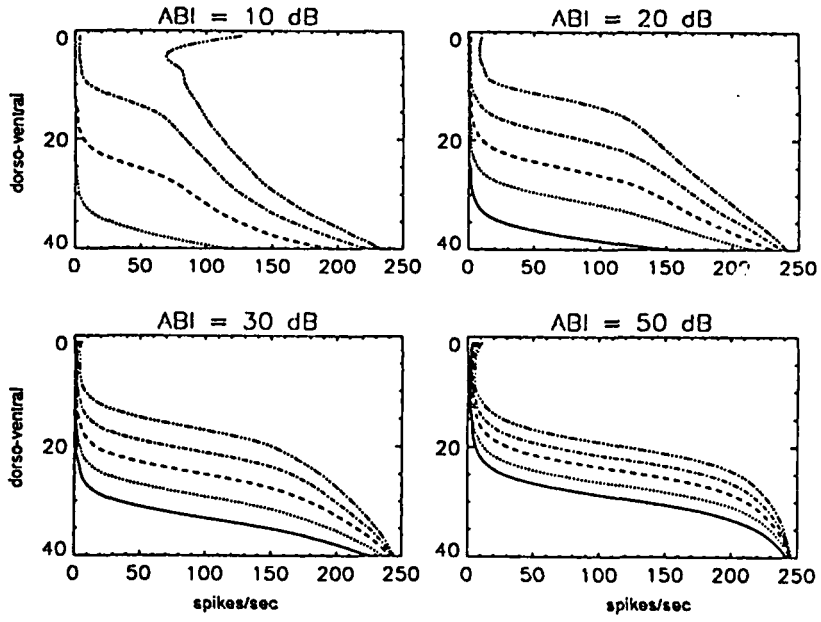


**Fig. 4.** Dorso-ventral patterns of activation in the VLVp. Each graph shows the response to 5 BID's for a fixed ABI. The y-axis is dorso-ventral depth (cluster number), with 0 corresponding to the dorsal surface. The BID's were -20dB (solid), -10dB (dotted), 0dB (dashed), 10dB (dot-dash) and 20dB (dot-dot-dot-dash). Note: for ABI=10dB, BID=+/- 20dB corresponds to monaural stimulation.

## ICL Model

The architecture of the ICL model is illustrated in Fig. 5. There are two ICL cell types, defined by their connectivity within the ICL, with the sensitive cells inhibiting the neighboring selective cells to one side along the medio-lateral axis. There is a topographic, point-to-point, inhibitory projection from the dorso-ventral axis of the VLVp onto the medio-lateral axis of the ICL (the orientation of which is arbitrary), which treats both cell types the same. NA projects onto the medio-lateral axis of the ICL in the same way it projects onto the dorso-ventral axis of the VLVp — uniformly to all cell types. The cells are grouped into 40 clusters along the medio-lateral axis, with 10 cells of each type in each cluster.

The patterns of stable stimulus-driven activity formed in the ICL are indicated by the stipling in Fig. 5. As it does in the VLVp, the NA input serves to uniformly activate all of the cells, independently of their position along the medio-lateral axis. The inhibitory projection from the VLVp squashes the activity in the ICL that cor-

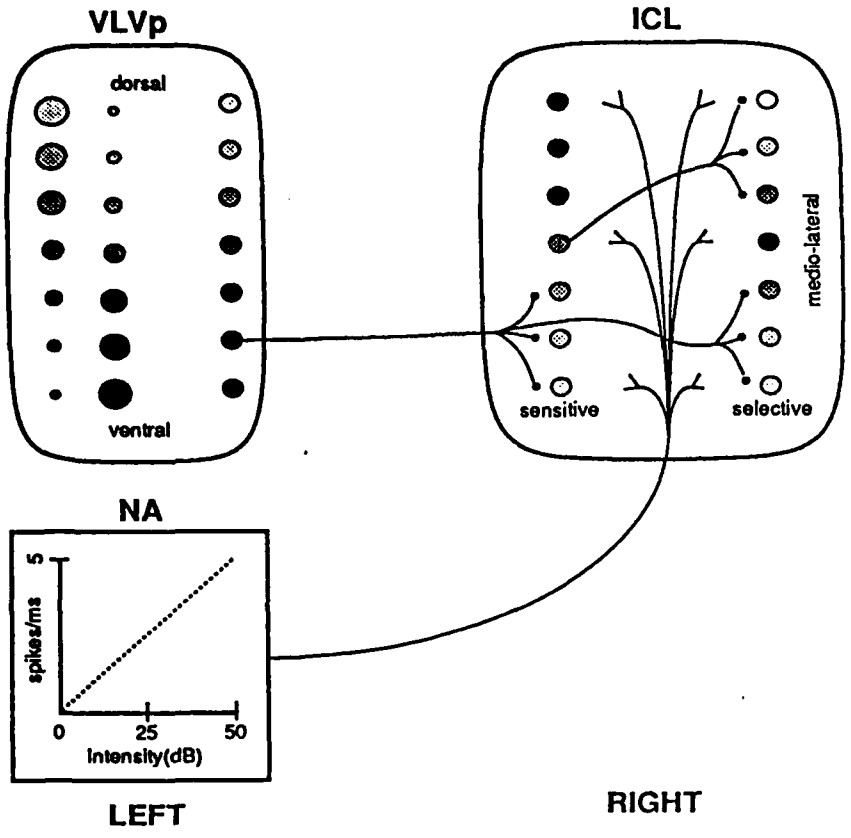


**Fig. 5.** ICL model architecture. The stipling within the cells indicates the degree of stimulus-driven activation (the darker the more active).

responds to the region of activity in the VLVp (ventral of the edge). This creates a wedge-like pattern of activation among the sensitive cells that is the complement of the pattern in the VLVp. The active sensitive cells then squash the activity in the corresponding selective cells. Only the selective cells in the position corresponding to the edge in the VLVp are free of heavy inhibition and remain active.

The dynamics of this pattern formation process are illustrated in Fig. 6. Note first that stable patterns are achieved in the ICL within the physiologically reasonable period of 6-10 ms. from stimulus onset (this does not include the response latency of NA itself). The rate limiting step in pattern formation is the feedback competition process in the VLVp. Such processes can be very slow to converge. An early version of the VLVp model [Spence and Pearson, 1990] that did not include the



local inhibitory cell class exhibited very slow convergence of roughly 60 ms. The local inhibitory class in the VLVp establishes a gradient of spontaneous activity, as seen in the 0 ms. panel in Fig. 6. This provides an intitial bias to the competition that prevents the dorsal neurons from getting excited at stimulus onset, excitation that would otherwise be slowly removed during the competition. These neurons also add negative feedback which increases the stability of the patterns. A gradient of spontaneous activity in the VLVp was reported in [Manley, *et al.*, 1988].

The model produces the desired response curves for the sensitive and selective cells, as shown in Fig. 7 (compare with graphs in Fig. 1). Their ABI dependence can be understood entirely in terms of the ABI dependence of the VLVp (The following discussion concerns the BID-selective cells. Similar arguments can be made for the sensitive cells). The position of the peak of activity along the medio-lateral axis in the ICL is directly determined by the position of the edge of activity along the dorso-ventral axis in the VLVp. Since the edge in the VLVp shifts with ABI (see Fig. 4), so will the peak in the ICL. This shift in the peak of the activation pattern corresponds to the shift in the response curves of those neurons with non-zero optimal BID (i.e., the neurons not positioned at the middle of the medio-lateral

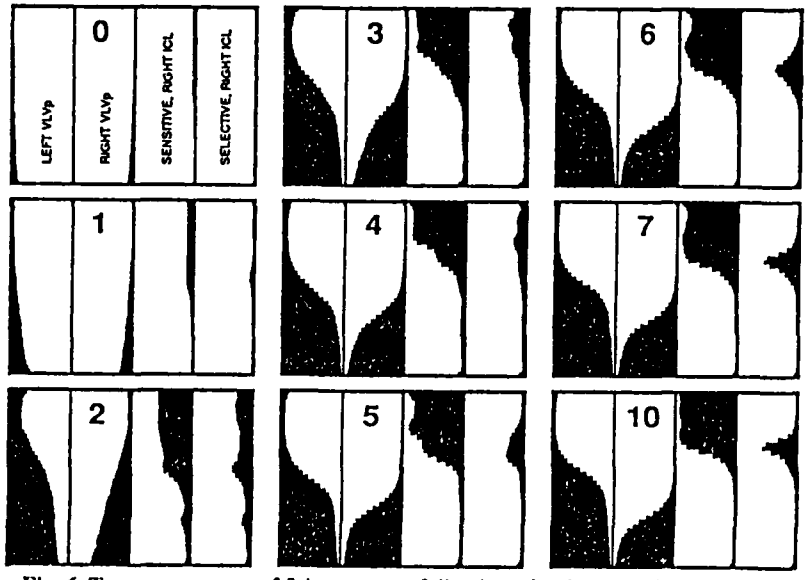


**Fig. 6.** Ten ms. sequence of firing patterns following stimulus onset in the left and right VLVp, and the BID-sensitive and BID-selective cells in the right ICL. The firing rates of the 40 cell clusters along the BID axis are depicted as a vertically oriented bar graph, with the bars pointing towards the left for all but the left VLVp, which point to the right. Frame "0" shows the spontaneous activity pattern prior to stimulus onset.

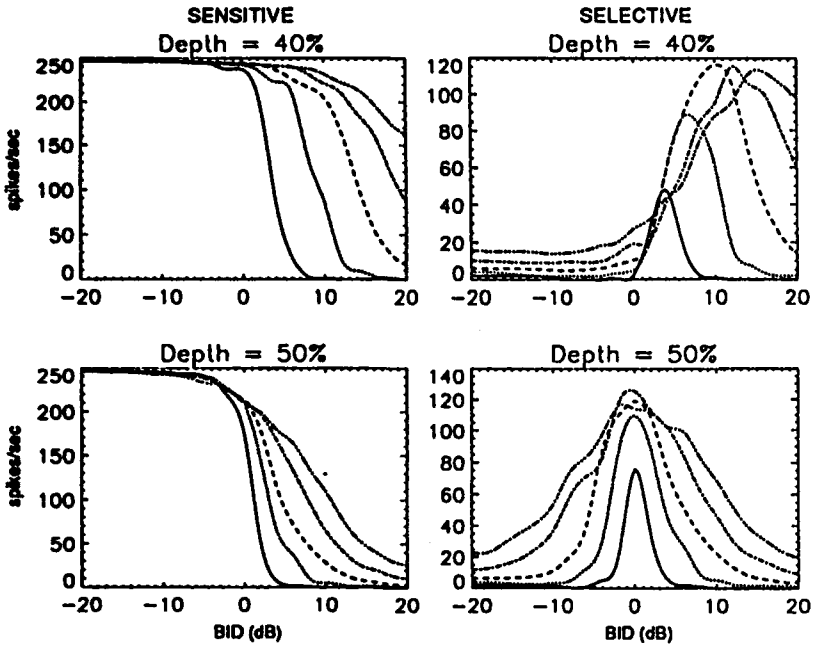


**Fig. 7. BID response curves of two sensitive (LEFT) and two selective (RIGHT) model ICL neurons, at positions (DEPTH) of 40% and 50% of the medio-lateral axis, for ABI's 10, 20, 30, 40 and 50 dB (solid, dot, dash, dot-dash, dot$^3$-dash).**

axis). The reduction in peak shift for a given change in BID caused by an increase in ABI (see Fig. 4 for the corresponding effect in the VLVp) corresponds to the broadening of the BID response curves.

The following procedure was used to measure the stable ongoing response to a given stimulus: 1. The output from NA was set to 0 spikes/sec and all neuronal potentials (eqn. 1) were set to their resting or leakage potentials; 2. The networks were simulated for 8 ms. with no stimulus present, enabling them to come to a quiescent equilibrium; 3. The stimulus was turned on for 80 ms. and the average firing rate of each cell was measured during the final 68 ms. period of the stimulus period (the first 12 ms. of the stimulus period was skipped to avoid transients).

The above procedure for measuring BID response curves assumes that there are no systematic shifts in the stimulus response during the 68 ms. period of spike averaging. Fig. 8 demonstrates that this assumption is valid. Such shifts do occur without the local inhibitory cell class within the VLVp, because of the slower convergence of the wedge-like patterns in the VLVp.

Fig. 8 also shows that there is a transient onset response in the VLVp and ICL model neurons, which is independent of BID, and which is more pronounced in the



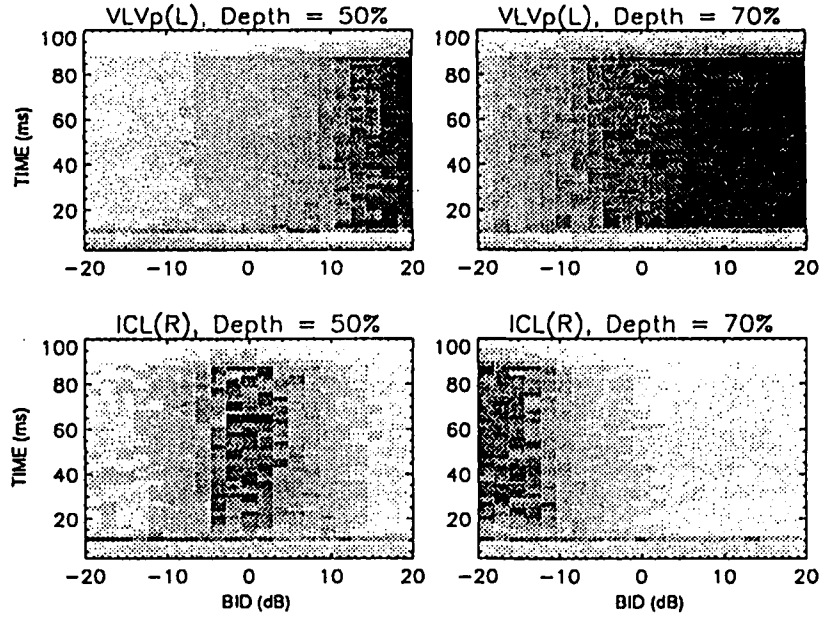


**Fig. 8. Firing rate as a function of BID and time, for neurons at positions 50% and 70% along the BID axis of the left VLVp and the right ICL. The darker the point the higher the firing rate. Stimulus onset and offset occured at 8 and 88 ms., respectively.**

ICL. These effects are due to the fact that the excitation from the NA is at first unchecked by inhibition. This effect is smaller in the VLVp due to the spontaneous activity which maintains a gradient of inhibition.

An earlier ICL model [Spence and Pearson, 1990] was based on the assumption that the output neurons of the VLVp were excitatory. However, recent unpublished work by R. Adolphs and I. Fujita has shown that ICL neurons are excited and inhibited by contralateral and ipsilateral stimulation, respectively. This implies that the VLVp input to the ICL must be inhibitory, and that the excitatory input must come from NA.

## VLVp Activity Modulation Experiment and Simulation

Recent experiments by R. Adolphs provided an indirect way of testing the VLVp and ICL models. In these experiments, the neural activity modulators lidocaine and bicuculline (BMI) were globally injected into one VLVp, while BID response curves were measured in the contralateral ICX. Given that the ICL is the predominant source of BID information to the ICX (see Fig. 1), it is likely that any observed changes in ICX BID-tuning would be the result of similar changes in in the ICL.

Preliminary tests showed that these drugs produced the expected effects in the VLVp — lidocaine reduced the firing activity through blocking action potential generation, while BMI increased the firing activity, through blocking the action of the inhibitory transmitter GABA-A. The effect of BMI within the VLVp was tested through the iontophoresis of 5mM BMI at a continuous 10 nA current. As shown in Fig. 9, there is a reversible increase in firing that is proportional to the normal firing level, and which is not BID specific. This behavior was recorded from 18 of 22 VLVp neurons.

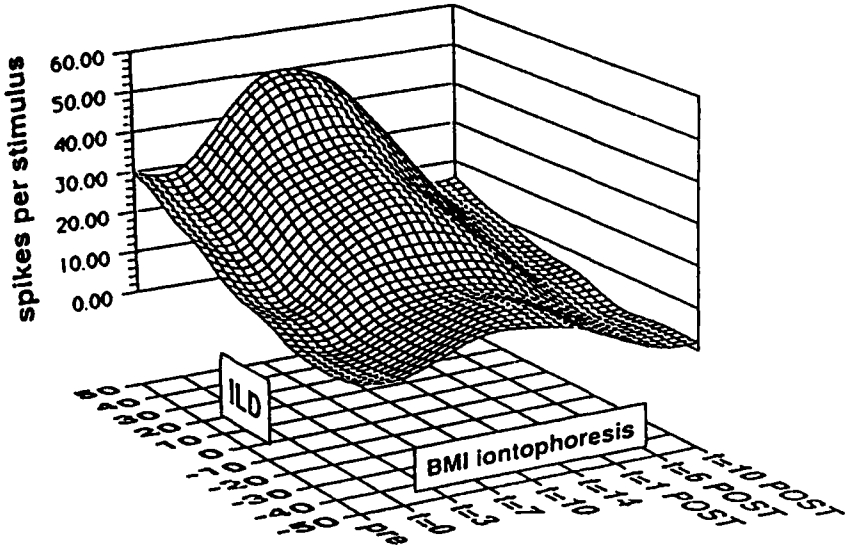


Fig. 9. Firing rate of a VLVp neuron as a function of BID (also known as ILD) before, during and after the iontophoresis of BMI.

The effects of global injections of lidocaine and BMI into the VLVp on the BID-curves of contralateral ICX neurons are shown in Fig. 10. The injections consisted of .2 microliters of a 5% xylocaine solution, or .2 microliters of a 5mM BMI solution. Lidocaine produces a reversible reduction in maximal response and a shift to lower optimal BID. BMI produces the opposite effect, in addition to a disproportionate increase in the response to greater than optimal BID's.

Similar changes are produced in the response of model ICL selective neurons, as shown in Fig. 11. Injections of lidocaine were simulated in the model by reducing the maximal firing rate of the "injected" VLVp to one-half that of the normal VLVp. The injection of BMI was simulated in the model solely by eliminating the inhibitory input from the local inhibitory cell class in the "injected" VLVp, without modifying the inhibition from the criss-cross cell class. This of course assumes that



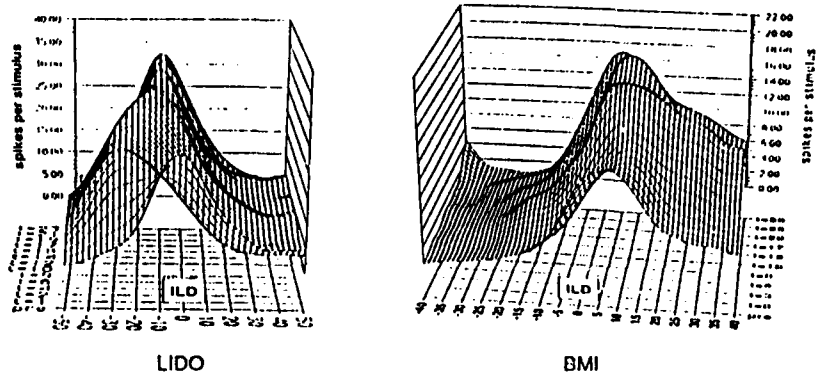


Fig. 10. BID (ILD) response curves from ICX neurons before, and following the global injection of lidocaine (LIDO) or bicuculline (BMI) into the contralateral VLVp.

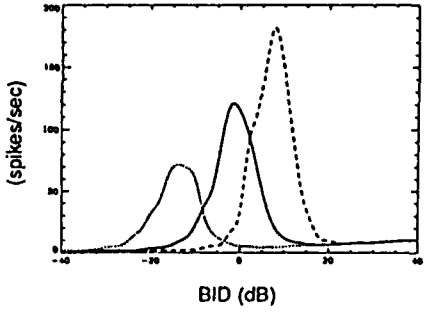


Fig. 11. BID-response curves of a model ICL selective neuron in its unperturbed condition (solid), and following simulated injections of lidocaine (dotted) and BMI (dashed) into the contralateral VLVp.

the local inhibitory class is GABAergic, while the criss-cross cells are not. This assumption is consistent with the results of [Carr, et al., 1989].

The effects of the injections can be simply understood in terms of the competitive balance between the two VLVp's. Injections of lidocaine into one VLVp will reduce the output of its criss-cross neurons, putting them at a competitive disadvantage. This will produce a ventral shift in the wedge-like pattern of the injected VLVp, and an equal dorsal shift in the other VLVp. These shifts in the VLVp will of course produce shifts in the peak-like patterns of the ICL, and corresponding shifts in the response curves of the BID-selective cells of the ICL. The model can not explain the disproportionate increase in the response to greater than optimal BID's under

the application of BMI. This effect could be due to perturbations to non-ICL inputs and processes, such as those from the medial shell and the process that generates ABI independence in the ICX.

## Summary

The network models presented here make many testable predictions and provide a framework for understanding the functional links between a host of seemingly unrelated physiological facts. The simulations demonstrate the neural plausibility of the qualitative spatial-derivative model of the origin of BID selectivity in the ICL. The models predict particular patterns of anatomical projections and neural circuitry. (1) NA projects uniformly along the BID axes of the VLVp and ICL. (2) The VLVp consists of three inhibitory cell classes, distinguished by their patterns of interconnection, their number density gradient, and their transmitter type. One class is non-GABAergic, projects in a criss-cross fashion to the contralateral VLVp, and its number density follows a dorso-ventral gradient, being high at the ventral end. A second class is GABAergic, connects locally, and its number density follows the opposite gradient from the criss-cross class. The third class is uniformly distributed along the dorso-ventral axis, and projects topographically onto the medio-lateral axis of the ICL. (3) The BID-sensitive cells of the ICL are inhibitory and connect to the neighboring BID-selective cells with greater BID thresholds. Temporally, the model predicts that the VLVp and ICL neurons have a short, BID-independent onset response, with the ICL transient being stronger. Future work will extend these models to include the broadly-tuned, BID-selective neurons in the ICL, the integration of the time and intensity pathways in the ICL, the projection from the ICL to the ICX, and the ABI independence of ICX neurons.

## Acknowledgements

This work was supported by AFOSR contract F49620-89-C-0131 and DARPA contract F49620-90-C-0010. We thank W. E. Sullivan, T. Takahashi and S. Volman for valuable technical discussions, and K. Miller for helpful suggestions concerning the presentation.

## References

Carr, C. E., I. Fujita, and M. Konishi (1989) Distribution of GABAergic neurons and terminals in the auditory system of the barn owl. *J.Comp. Neurol.* 286:190-207.

Fujita, I. and M. Konishi (1989) Transition from single to multiple frequency channels in the processing of binaural disparity cues in the owl's midbrain. *Soc. Neurosci. Abstracts* 15:114.

Haresign, T. and A. Moiseff (1988) Early growth and development of the common barn-owl's facial ruff. *The Auk*, 105:699-705.



Knudsen, E. I. (1984) Synthesis of a neural map of auditory space in the owl. In *Dynamic Aspects of Neocortical Function*, G. M. Edelman, W. E. Gall and W. M. Cowan, eds., Wiley, New York.

Manley, G. A., C. Köppl, and M. Konishi (1988) A neural map of interaural intensity differences in the brain stem of the barn owl. *J. Neurosci.* 8:2665-2676.

Moiseff, A. (1989) Binaural disparity cues available to the barn owl for sound localization. *J. Comp. Physiol.* 164:629-636.

Payne, R. S. (1971) Acoustic localization of prey by barn-owls (Tyto alba). *J. Exp. Biol.* 54: 535-573.

Spence, C. D. and J. C. Pearson (1990) The computation of sound source elevation in the barn owl. In *Advances in Neural Information Processing Systems 2*, D. S. Touretzky, ed., Morgan Kaufmann, San Mateo, CA. .

Spence, C. D. and J. C. Pearson (1991) Models of the computation of sound elevation in the barn owl. In *Analysis and Modeling of Neural Systems*, F. Eeckman, ed., Kluwer, Boston.

Spence, C. D. and J. C. Pearson (1992) A resonance model of high frequency binaural phase sensitivity in the barn owl's auditory brainstem. In *Analysis and Modeling of Neural Systems II*, F. Eeckman, ed., Kluwer, Boston.

Sullivan, W. E. and M. Konishi (1984) Segregation of stimulus phase and intensity coding in the cochlear nucleus of the barn owl. *J. Neurosci.* 4:1787-1799.

Takahashi, T. T. (1988) Commissural projections mediate inhibition in a lateral lemniscal nucleus of the barn owl. *Soc. Neurosci. Abstracts* 14:323.

Takahashi, T. T. and M. Konishi (1988) Projections of the cochlear nuclei and nucleus laminaris to the inferior colliculus of the barn owl. *J. Comp. Neurol.*, 274:190-211.

Takahashi, T. T. and M. Konishi (1988) Projections of nucleus angularis and nucleus laminaris to the lateral lemniscal nuclear complex of the barn owl. *J. Comp. Neurol.*, 274:212-238.

Wagner, H., Takahashi, T. and M. Konishi (1987) Representation of interaural time difference in the central nucleus of the barn owl's inferior colliculus. *J. Neurosci.*, 7:3105-3116.